Journal of Materials Chemistry C

Accepted Manuscript

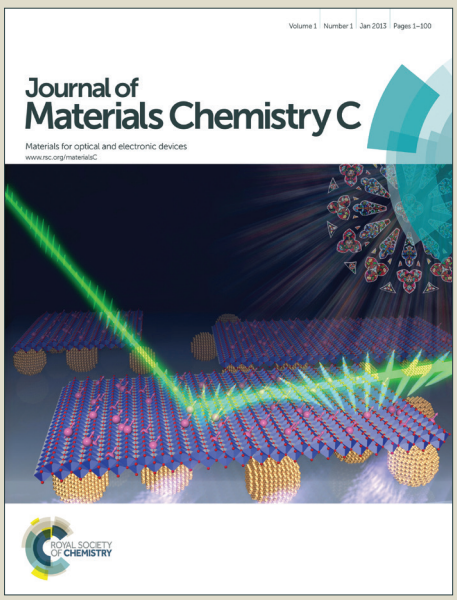

ROYAL SOCIETY OF CHEMISTRY

www.rsc.org/materialsC

Structural, optical, magnetic and half metallic studies of cobalt doped ZnS thin films deposited by chemical bath deposition

Muhammad Saeed Akhtar[a,b], Yousef G. Alghamdi[c], Mohammad Azad Malik[a*], Rana Muhammad Arif Khalil[d], Saira Riaz[b], Shahzad Naseem[b]

[a]School of Materials, The University of Manchester, Oxford Road, Manchester M13 9PL, U.K.

[b]Centre of Excellence in Solid State Physics, University of the Punjab, Lahore-54590, Pakistan.

[c]Faculty of Science & Art –Rabigh, King Abdulaziz University, Jeddah- Saudi Arabia.

[d]Department of Physics, Sahiwal sub-campus, Bahauddin Zakariya University, 57000, Pakistan.

*Corresponding Author

Mohammad Azad Malik

E-mail: azad.malik@manchester.ac.uk

ABSTRACT

The results of experimental and theoretical study on structural, optical, magnetic and half metallic properties of cobalt doped ZnS thin films deposited by chemical bath deposition are presented. Phase pure deposition of cubic ZnS with slight variation in lattice constant due to incorporation of cobalt in ZnS lattice is observed. It is shown that the crystallite size calculated by Scherrer equation has an average value of 12 nm. The agglomeration of nanocrystallites leads to the formation of spherical clusters having an average diameter of 170 nm onto the substrate surface. Room temperature ferromagnetism in cobalt doped ZnS thin films depending on cobalt concentrations is observed. Such behavior corresponds to the dopant induced magnetism in the host semiconductor and agrees well with the theoretical predictions in addition to the observation of half metallicity. The variation in band gap as a function of cobalt concentration attributes to the structural modification after cobalt doping and occurrence of quantum confinement phenomenon. Photoluminescence emission characteristics of the samples present the formation of luminescence centers of cobalt ions causing the radiative recombination processes. The increased intensity of PL emissions indicating that the concentration quenching effect did not appear up to the doping concentration of 12 at.% .

Keywords: Chemical bath deposition; ZnCoS; Thin films; p-XRD; Magnetic properties; Band gap

1. INTRODUCTION

ZnS based dilute magnetic semiconductors are highly desired in spintronic devices having dual functionality taking into account the spin degree of freedom along with electronic charge to achieve new functionalities in the devices. High data processing speed, high integration density, low power consumption and non-volatility of such devices make the difference in contrast to conventional devices working on electronic charge only.

The cobalt doped ZnS in the form of thin films is the least investigated material regarding magnetic studies. Literature survey showed that there are only few reports on the study of cobalt doped ZnS thin films. In 2011, deposition of cobalt doped ZnS thin films by spray pyrolysis[1] was reported without depositing the pure phase of ZnS first. The films were proved to be cobalt doped zinc oxysulfide instead of zinc cobalt sulfide. In 2012, a study was published regarding the deposition of hexagonal cobalt doped ZnS thin films *via* pulsed laser deposition,[2] and the growth of cobalt doped ZnS nanoparticles by colloidal method with investigation of optical and magnetic properties.[3-7] Other methods to deposit/synthesize doped ZnS films and nano crystals include; aqueous method,[6] chemical bath deposition,[7, 8] refluxing technique,[9] precipitation method,[10, 11] pulsed laser ablation,[12] solid state reaction method,[13] solvothermal technique[14] and hydrothermal method,[15, 16] aerosol assisted chemical vapour deposition and colloidal thermolysis[17-24]. Among these, CBD is the most simple and cost effective method to synthesize thin films and nano crystals. The only report found on cobalt doping in ZnS *via* CBD is presented by Tang *et al.*[7] showing the enhancement in efficient ultraviolet emission of ZnS nano spheres after cobalt doping.

Theoretical investigations on cobalt doped ZnS clusters have also been carried out earlier.[25-27] Unfortunately, many experimental and theoretical findings regarding magnetic properties of

such materials are contradictory showing spin glass or anti-ferromagnetic, paramagnetic and ferromagnetic behaviors.

In this work, we present the optimized growth of cobalt doped nanocrystalline ZnS thin films on glass substrates by CBD method. The structural, morphological, magnetic and optical properties of deposited thin films have been studied. Theoretical (DFT) calculations on cobalt doped ZnS cubic zinc-blende clusters are also part of this work.

2. EXPERIMENTAL SECTION

2.1 Chemicals:

All reagents, zinc chloride, cobalt chloride, thioacetamide and urea were purchased from Sigma-Aldrich and used without further purification. De-ionized water was used as solvent in all experiments. Acetone, Isopropyl alcohol and ethanol were used for cleaning of the substrate.

2.2 Instruments:

CBD experiments were carried out in jacketed beakers connected to thermostat water bath. Mettler Toledo meter which was calibrated against standard pH 2.00, 4.01, and 7.00 buffers was used to record pH. Bruker D8 advance Diffractometer with Cu-Kα radiation was used for X-ray powder diffraction measurements. XRD data was recorded across a 2θ range of 20 to 80° for three hours and twenty minutes scan using a step size of 0.02°. SEM and EDX analyses were carried out using Philips XL 30 microscope. TEM, HRTEM and SAED images were collected using Tecnai 20 F30 transmission electron microscope with accelerating voltage of 200 kV. Lake Shore's 7407 Vibrating Sample Magnetometer was used to obtain magnetic measurements of these cobalt doped ZnS thin films. The absorbance and transmittance spectra were acquired using

Agilent HP 8453 UV-Vis spectrophotometer. Photoluminescence data was taken by Fluorolog 22, HORIBA PL. The density functional calculations were carried out using Elk-code.

2.3 Synthesis of cobalt doped ZnS thin films:

The cobalt doped ZnS thin films were deposited onto glass substrates in a chemical bath containing solutions of zinc chloride (0.15 M), cobalt chloride (0.15 M), urea (5 M) and thioacetamide (1 M). All the solutions were prepared in de-ionized water separately. Urea solution was added to the solution of zinc chloride to start the hydrolysis followed by addition of cobalt chloride solution in appropriate amounts to achieve desired doping levels of 3, 6, 9 and 12%. Finally, solution of thioacetamide was added and the mixture was stirred vigorously to achieve homogeneous mixing of precursors. The pH of solution was adjusted to 3.8 by drop wise addition of 0.2 M HCl. The reaction mixture was then transferred to a jacketed beaker attached with a thermostat bath and maintained at a temperature of 80 °C along with uniform magnetic stirring. After ten minutes of reaction at 80 °C, the transparent solution started turning milky turbid. Glass substrates (1.5×2.5 cm^2) degreased with ethanol and ultrasonically cleaned with acetone/isopropyl alcohol were immersed vertically in the chemical bath. Substrates were removed from the bath after 3, 3.15, 3.30 and 3.45 hours and washed with de-ionized water. It is important to mention here that, deposition time of extra 15 minutes was given to samples as cobalt concentration increased in order to control the morphology and to obtain the grain size of almost equal size for all four cobalt concentrations of 3, 6, 9 and 12 %, respectively. Precipitates and loosely adhered particles on the substrate were removed by sonication. The films were allowed to dry under nitrogen stream before further characterizations.

3. COMPUTATIONAL DETAILS

Full Potential Linearized Augmented Plane Wave (FPLAPW) approach was used to solve Kohn-Sham equation within Density Functional Theory [28, 29] formulation as is employed in the Elk-code in order to investigate the electronic and magnetic properties of $Zn_{1-x}Co_xS$ alloys. Generalized Gradient Approximation plus PBE [30] along with Hubbard functional U (GGA-PBE+U) was used for optimization of the exchange correlation energy. Inside the non-overlapping spheres surrounding the atomic sites (muffin-tin spheres) the wave functions were expanded into spherical harmonics with angular momentum quantum number lmax = 10 and in the interstitial region, wave functions are expanded into plane wave basis. A plane wave cutoff of rgkmax = 7 was used for the expansion of wave functions inside the interstitial regions. The cutoff for reciprocal vector of Fourier expansion i.e. gmaxvr was set to 14 and actual value for smearing, 'swidth' = 0.001. Maximum 'G' for potential and density was fixed at 12. Maximum angular momentum used for APW functions was 8 and effective Wigner radius was fixed to 0.65 Å. The muffin-tin radii RMT's were fixed at value of 1.058 Å so that there is no charge leakage from the core and total energy convergence is ensured. Spin orbit coupling was considered to observe spin polarization. Complex Hermitian eigen solver was used since the crystal has no inversion symmetry. A dense uniformly distributed mesh of 4×4×4 k-points was used in the irreducible part of Brillouin Zone ensuring that the Brillouin Zone is densely populated. The core electrons were treated fully relativistically by solving the Dirac equation, whereas the valence electrons were treated non-relativistically. Furthermore, we have included the structure optimization to relax the inter-atomic positions upon deformations.

4. RESULTS AND DISCUSSION

Figure 1 reveals the camera images of synthesis (on left) and glass substrates (on right) after deposition of cobalt doped ZnS thin films with different cobalt concentrations. It is bit difficult to differentiate visually between different deposits since color (off-white) of the samples didn't vary too much with increasing concentration of cobalt.

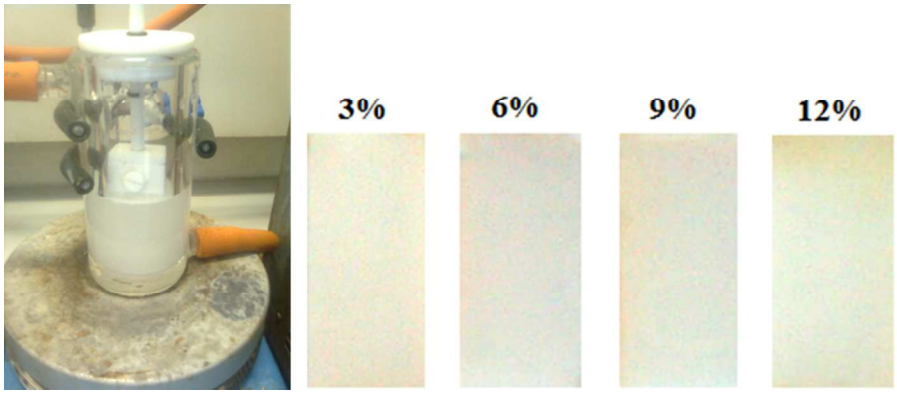

Figure 1: Camera pictures of cobalt doped ZnS synthesis (left) and thin films deposited onto glass substrates (right) with different concentration of cobalt precursor into the chemical bath.

4.1 Structural Studies

The structural study was performed by X-ray diffraction technique. p-XRD patterns (Figure 2) show the polycrystalline nature of cobalt doped ZnS thin films. The observed diffraction peaks are broad due to the nano size of deposited crystallites. The peaks along (111), (220) and (311) lattice planes correspond to the standard pattern of cubic ZnS (ICCD # 01-005-0566). Effect of cobalt incorporation in ZnS is evident from shift of diffraction peak corresponding to (111) plane from standard 2θ of 28.86° to bit higher values, since the ionic radius of Co^{+2} (0.72 Å) is bit smaller than that of Zn^{+2} (0.74 Å). The shift of diffraction peak (111) is also shown in Figure 2. A slight change in lattice constant was observed but the structure remains cubic and not

tailored by the addition of different amounts of cobalt into the ZnS lattice at least up to the detection level of p-XRD [8]. Substitution of cobalt into the ZnS lattice is evident by the absence of any peaks corresponding to either cobalt, cobalt sulfide or any other impurity. The Full Width at Half Maximum (FWHM) of p-XRD peaks for all the samples have almost same value revealing that the deposited thin films comprised of crystallites with almost equal sizes.

The Crystallite size calculated by Scherrer equation for the cobalt doped thin films has an average value of 12 nm. The value of lattice parameter 'a' after doping is found to be smaller (5.382 to 5.306 Å) than that of pure ZnS (5.406 Å). The observed decrement in lattice constant is close enough to the reported data in limitations to the expected change in structure of ZnS due to cobalt doping. The variation in lattice constant as a function of dopant's concentration is shown in Figure 3.

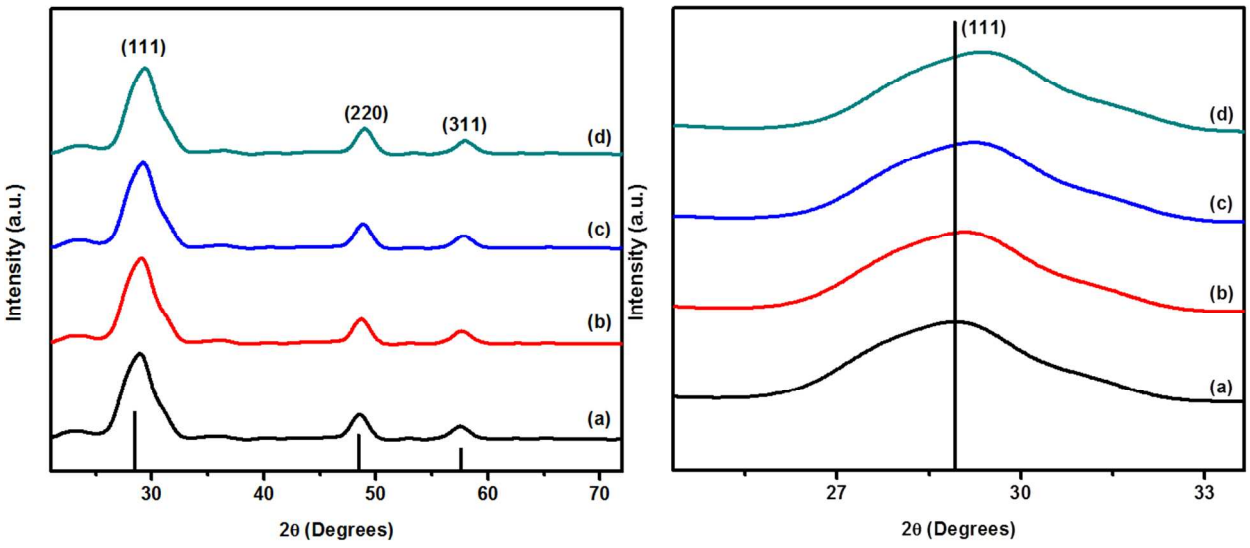

Figure 2: p-XRD patterns of cobalt doped ZnS thin films (a) 3% Co, (b) 6% Co, (c) 9% Co and (d) 12% Co. Vertical lines on X-axis represent the standard pattern of ZnS. The shift in 2θ value for major peak (111) is shown on right.

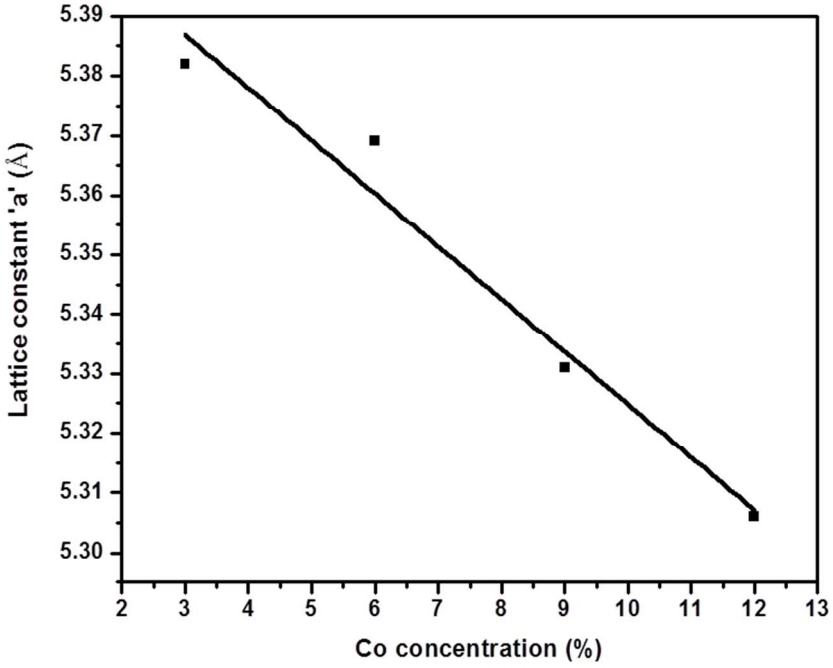

Figure 3: Variation in lattice constant as a function of cobalt concentration

4.2 Morphological Studies

The morphology of cobalt doped ZnS thin films was observed through SEM micrographs. SEM representative images (Figure 4) of the ZnCoS thin films show distribution of almost spherical nanoparticles on the surface of substrates. It was observed that agglomeration of nanocrystallites leads to the formation of spherical clusters having an average diameter of 170 nm onto the substrate surface. The uniform growth of ZnS on glass substrates has been explained earlier [31]. Size distribution of particles was analyzed by an image analysis program (ImageJ) and average diameter of the particles was found to be 170 ± 10 nm (Figure 5).

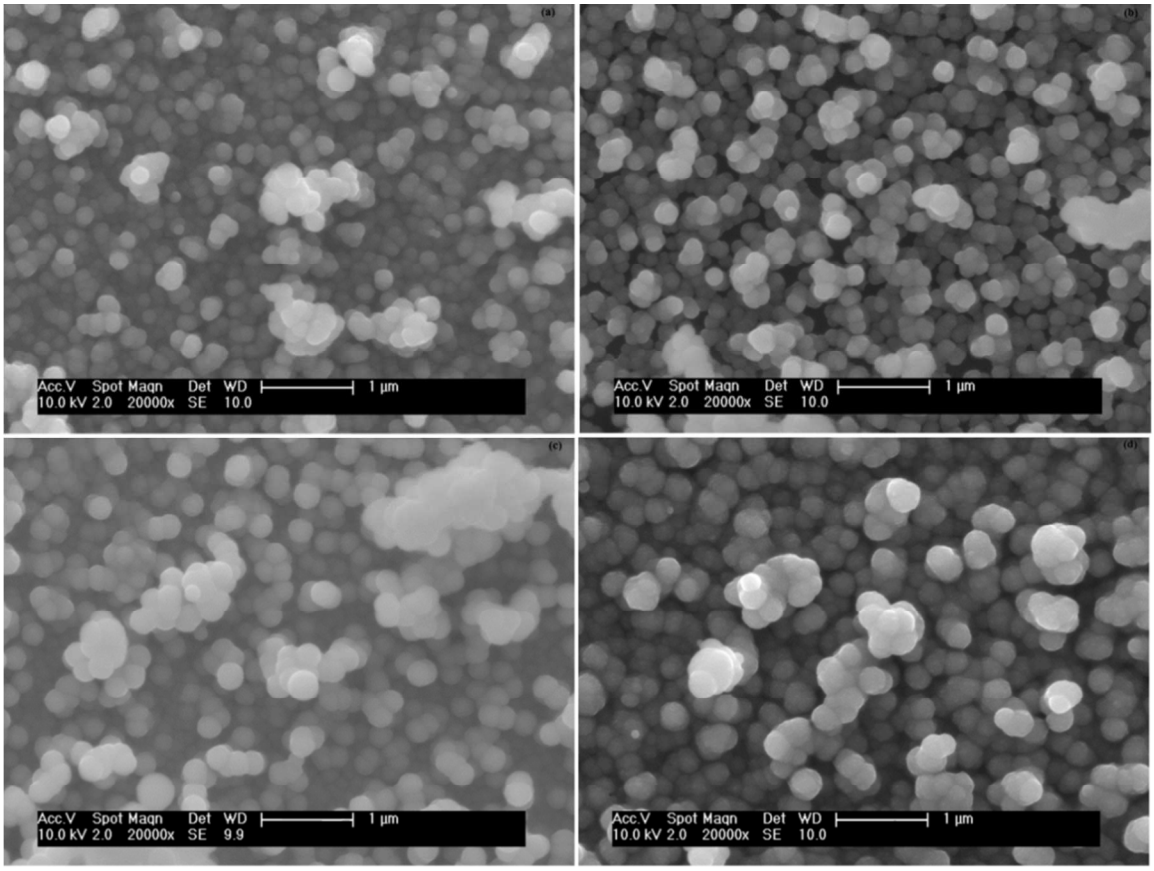

Figure 4: SEM images of cobalt doped ZnS thin films after addition of (a) 3% Co, (b) 6% Co, (c) 9% Co and (d) 12% Co

The presence of cobalt in ZnS was confirmed by EDX analysis. The amount of dopant (cobalt) added in precursors was slightly greater than the amount found in EDX analysis. For comparative study, the amount of cobalt in ZnS matrix obtained experimentally would have almost equal value as used for theoretical calculations. The atomic ratios of cobalt extracted through EDX analysis were found to be 3.129247, 6.245236, 9.366940 and 12.53188 at. %. Glass constituents such as, silicon, sodium, calcium, magnesium, potassium and aluminum were also detected in EDX spectrum because of the thin nature of films. The atomic ratios of zinc, cobalt and sulfur obtained from EDX measurements are presented in Table 1.

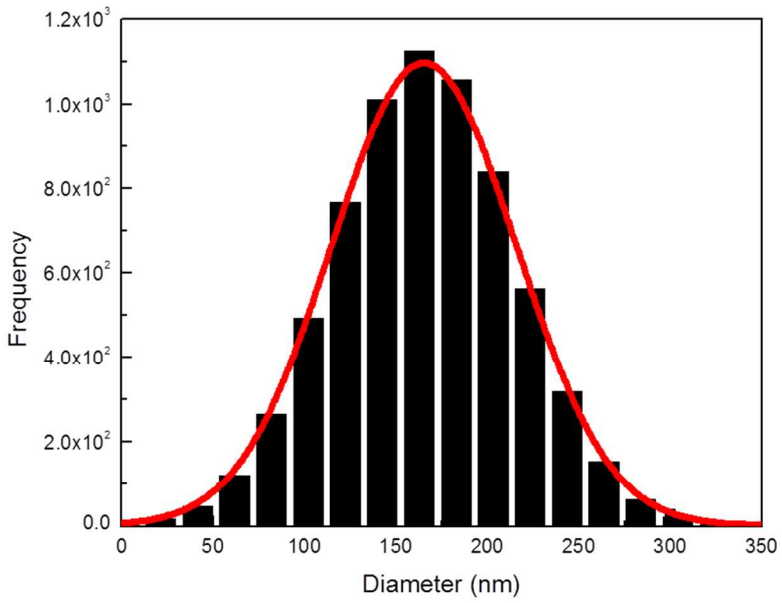

Figure 5: Particle size distribution of ZnCoS thin films

Table 1: Atomic percentage of zinc, cobalt and sulfur in ZnS:Co thin films

EDX analysis	3% Co	6% Co	9% Co	12% Co
Element	**at. %**	**at. %**	**at. %**	**at. %**
Zinc	47.84327	46.98734	43.88581	40.99199
Cobalt	3.129247	6.245236	9.366940	12.53188
Sulfur	49.02748	44.76743	46.74725	46.47612

Microstructure of cobalt doped ZnS thin films was also studied in detail with the help of transmission electron microscopy (TEM), high resolution transmission electron microscopy (HRTEM) and selected area electron diffaraction (SAED). TEM images of ZnCoS thin films, show the clusters of nanoparticles (Figure 6). HRTEM image (Figure 6b) confirms the crystalline nature of the ZnCoS thin films. Inter planner spacing (0.30 Å) calculated

experimentally is in fair agreement with that expected for (111) plane of cubic phase of ZnS after decrement in lattice spacing due to cobalt incorporation. SAED pattern (Figure 6c) shows a set of three circular rings obtained due to diffraction of electrons from (111), (220) and (311) planes of cubic ZnS. SAED pattern thus indicates polycrystalline nature of ZnCoS thin film.

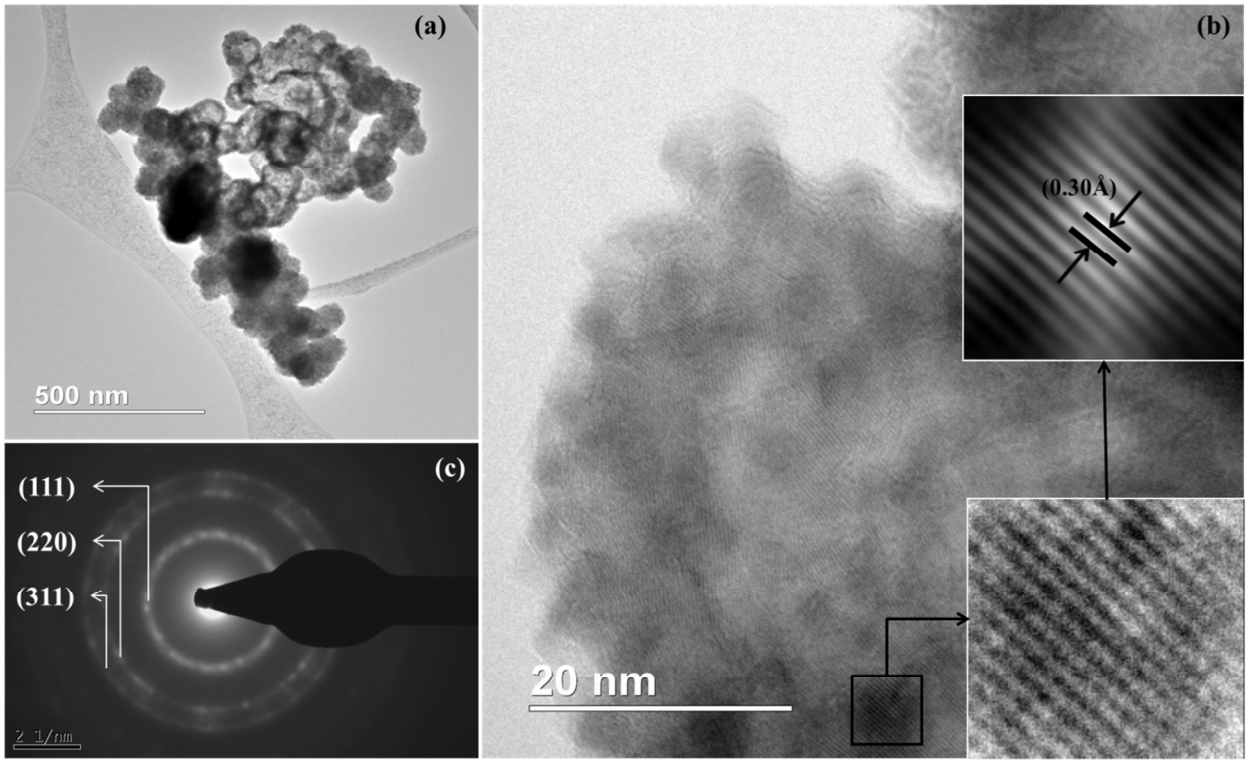

Figure 6: TEM images for the ZnCoS thin film with cobalt concentration of 6%

4.3 Optical Studies

Optical band gap of cobalt doped ZnS thin films was determined by extrapolating linear part of the $(\alpha h\upsilon)^2$ Vs $h\upsilon$ curve to the energy axis, when $(\alpha h\upsilon)^2 = 0$. The average value of band gap was found to be 3.6 eV. A slight increment in the value of band gap energy is observed with increasing cobalt concentration. This increment might be attributed to the structural modification after cobalt doping and occurrence of quantum confinement phenomenon when the crystallites are small enough. The variation of $(\alpha h\upsilon)^2$ with photon energy $h\upsilon$ is shown in Figure 7 representing the direct type of transitions. The optical energy gap 'Eg' and absorption coefficient 'α' are related by the Tauc's relation.[32]

$$\boldsymbol{\alpha = \left(\frac{k}{h\upsilon}\right)(h\upsilon - E_g)^n} \qquad (1)$$

Where k is a constant, h is Planck's constant, $h\upsilon$ is the incident photon energy and n is a number which characterizes the nature of electronic transition between valence band and conduction band. For direct allowed transitions n =1/2, therefore the formula used is:

$$\boldsymbol{\alpha = \left(\frac{k}{h\upsilon}\right)(h\upsilon - E_g)^{\frac{1}{2}}} \qquad (2)$$

This on further simplification gives:

$$\boldsymbol{\frac{1}{C}(\alpha h\upsilon)^2 = h\upsilon - E_g} \qquad (3)$$

The inset of Figure 7 shows the change in spectral transmittance of cobalt doped ZnS thin films at room temperature. It is found that all the films are highly transparent in the visible region of optical spectrum. The transmittance observed is in the range of 60-80%. The transmittance of ZnS thin films decreases slightly with increasing cobalt concentration that might be due to increase in crystallinity and densification of the films. This decrease in transmittance would also be the result of increased surface roughness as the crystallinity increases.[33]

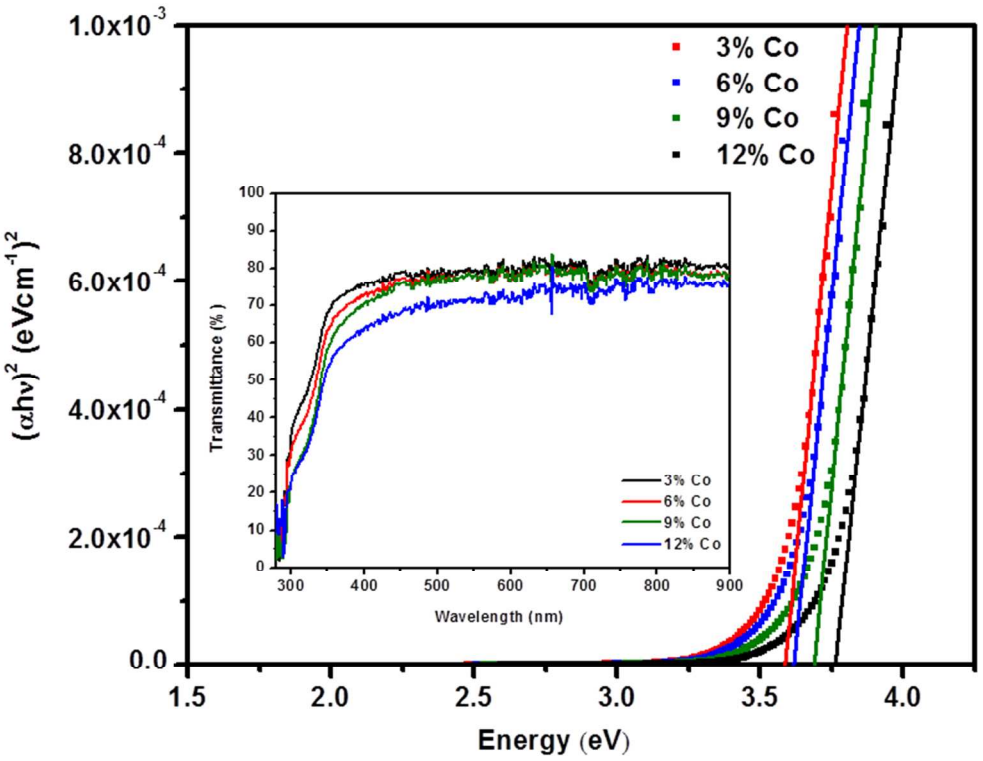

Figure 7: Band gap and transmission plots of cobalt doped ZnS thin films at different cobalt concentrations

Room temperature photoluminescence spectra of cobalt doped ZnS thin films are shown in Figure 8. The PL spectra of thin films excited at 340 nm show two emission bands at 380 and 510 nm. The emission at 380 nm result from transition of electrons from shallow states near conduction band to the sulfur vacancies present near the valence band in ZnS lattice while the emission at 510 nm is attributed to the characteristic of cobalt. The luminescence centers of cobalt ions are formed when cobalt is incorporated into the ZnS host lattice. Since Co^{+2} is a sensitizing agent and hence its presence in the host lattice would enhance the radiative recombination processes[34, 35]. With the increase in doping concentration, the luminescence centers substantially increases which are then responsible for significant increase in PL intensity of green emission at 510 nm. Hence from the PL emission spectra, it might be concluded that the Co ions are incorporated successfully into the ZnS lattice as expected in agreement

with the p-XRD results (Figure 2). The increased intensity of PL emissions indicating that the concentration quenching effect did not appear up to the doping concentration of 12 at.% in contrast to previously reported decay in photoluminescence intensity at cobalt concentration of 5 at.% [16]. This observation reveals that cobalt ions substituted the zinc ions even at higher doping concentration of 12 at.% rather than staying at the surface or at interstitial positions. It is very interesting that cobalt dopant can effectively enhance the intensity of green emission.

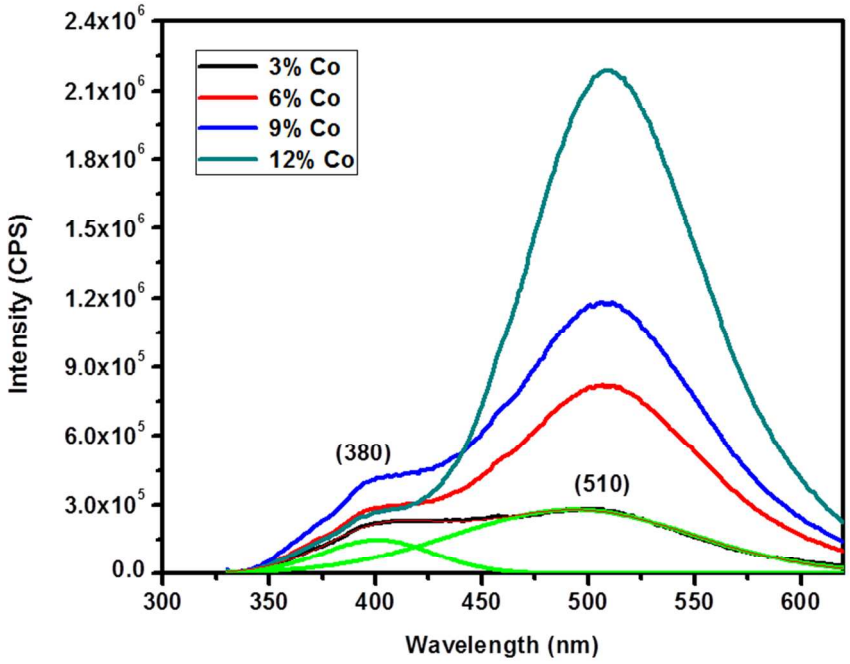

Figure 8: PL spectra of cobalt doped ZnS thin films at different cobalt concentrations

4.4 Magnetic Studies

Vibrating sample magnetometer was used to study the magnetic properties of ZnCoS thin films. The M-H curves obtained for all the samples are shown in Figure 9. Hysteresis loop with negligible values of ramanance and retentivity was observed for cobalt concentration of 3 at.% but well-defined hysteresis loops were observed as an evidence of room temperature ferromagnetism for higher cobalt concentrations. The XRD and HRTEM show single phase deposition of cobalt doped ZnS thin films, hence it would be speculated that ferromagnetism

above room temperature originates from the single crystals of ZnCoS nanoparticles. The observed findings are in close agreement with the results reported earlier [6]. Thus it would be considered that substitution of cobalt in ZnS lattice results in the ferromagnetic coupling state without changing the crystal structure which implies that this may be carrier induced ferromagnetism further confirmed by DFT calculations.

The coercivity is observed to be invariable with cobalt concentrations of 6-12 at.% having value of 293 Oe. The hysteresis loop of the sample with 3% of cobalt to be saturated, for the applied field of 9 kOe. Further increase in cobalt concentration, showed systematic increase in the value of saturation magnetization. This systematic increment in magnetization may be due to introduction of ferromagnetic ordering with increasing cobalt concentration in ZnS thin films. The retentivity for 6 at.% concentration of cobalt is 9.33×10^{-4} emu and is observed to increase for 9 and 12 at.% of cobalt concentration to 1.08×10^{-3} emu.

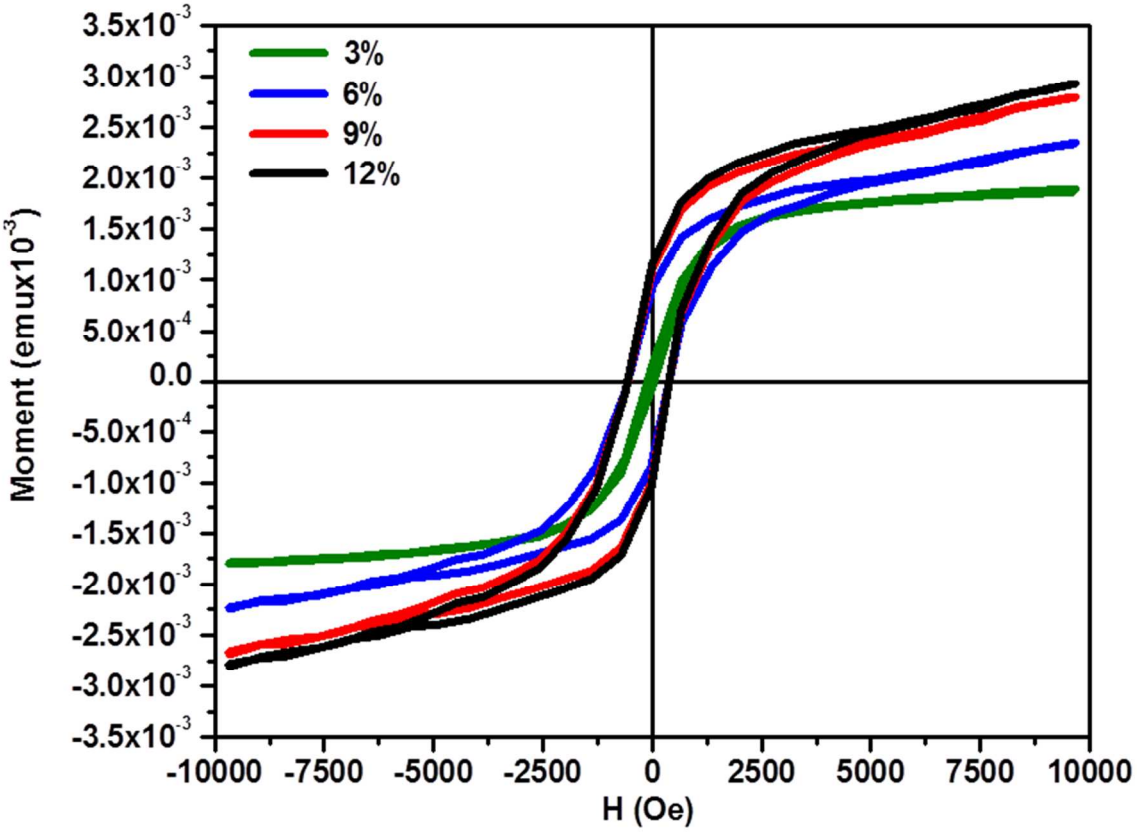

Figure 9: M-H curves of ZnCoS thin films with different cobalt concentrations

4.5 Theoretical Investigations

To further investigate the effect of cobalt doping, origin of magnetism and half metallicity, DFT calculations using Elk-code have been performed. The DFT calculations on cobalt doped ZnS were performed by using 64 atom supercells with 32 atoms each for zinc and sulfur. For comparative study the doping concentration selected for DFT calculations were almost the same as used in the experiment. Figure 10 shows the cobalt doped ZnS supercells. The white, yellow and red spheres in Figure 10 represent the zinc, sulfur and cobalt atoms, respectively.

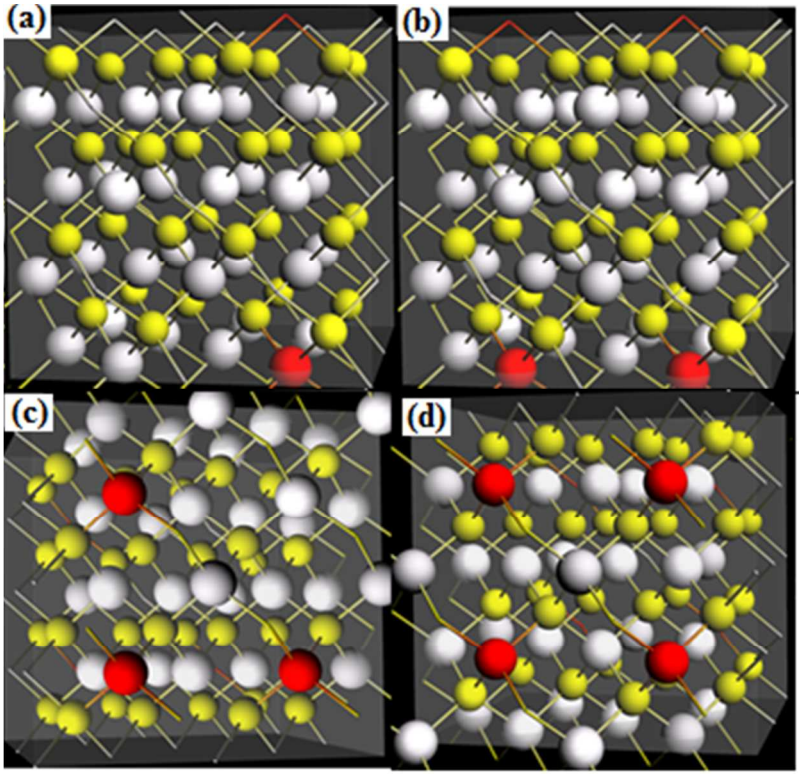

Figure 10: Supercells (2×2×2) of cobalt doped ZnS (a) 3.125% Co, (b) 6.25% Co, (c) 9.375% Co and (d) 12.50% Co

The lattice constants were optimized after geometry relaxation. A slight decrement in lattice parameters was observed in comparison to the experimentally reported value of 5.416 Å [36, 37], since there is small difference in ionic radii of zinc (0.74 Å) and cobalt (0.72 Å). In order to compare the energetic stability of cobalt doped ZnS, we have calculated the formation energies for all doping concentrations. It was observed that the formation energy of cobalt doped ZnS (-2.2183 eV/atom) for doping concentration of 12.50 at.% is a bit less than that with doping concentration of 3.125 at.% (-2.0812 eV/atom) due to exothermic nature of reaction (Figure 11). Energy minimization was done by slight variation in lattice parameters of ZnS after cobalt incorporation. The variation in theoretically calculated lattice parameters as a function of cobalt concentration is shown in Figure 12.

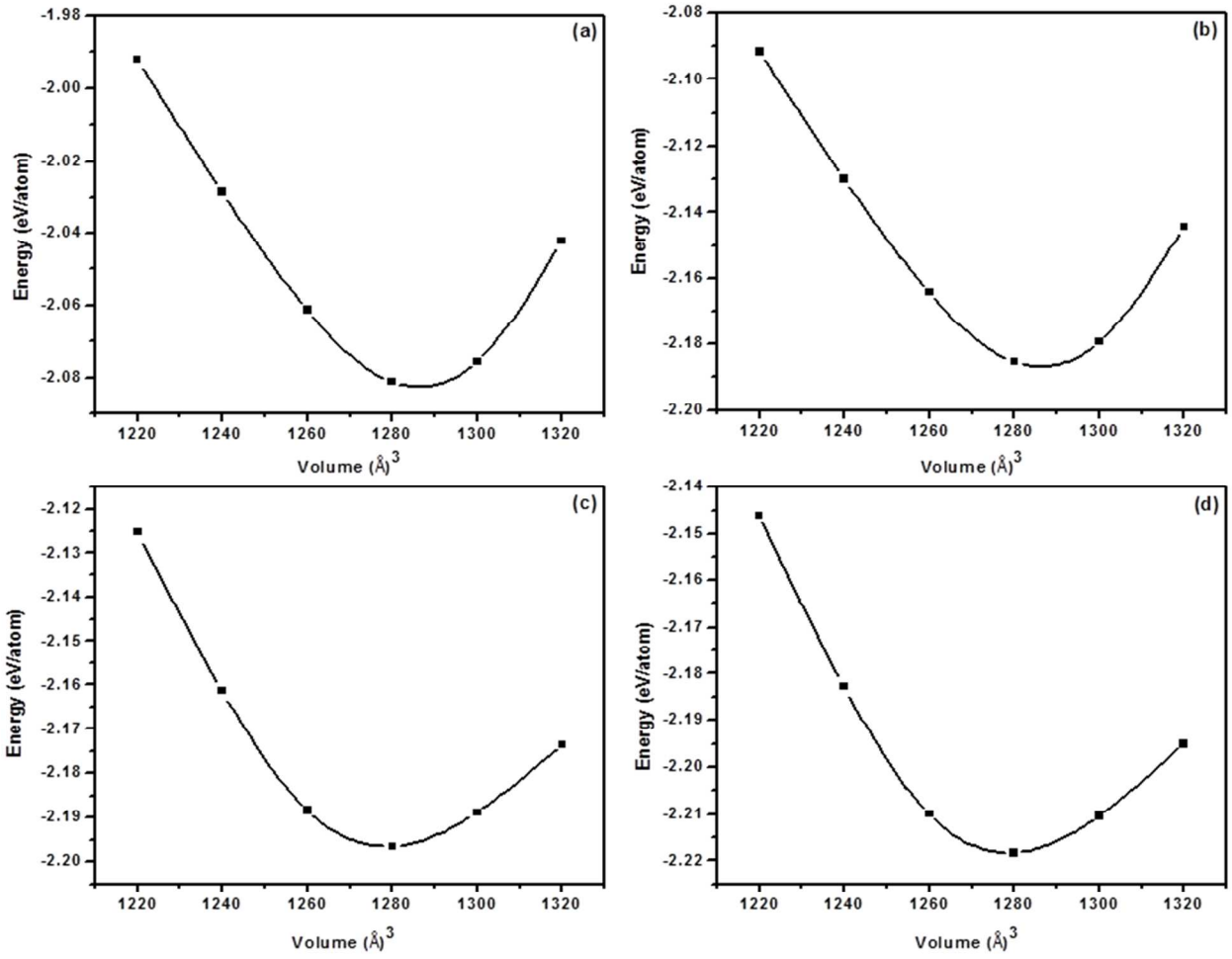

Figure 11: Energy Vs volume curves for cobalt doped ZnS (a) 3.125% Co, (b) 6.25% Co, (c) 9.375% Co and (d) 12.50% Co

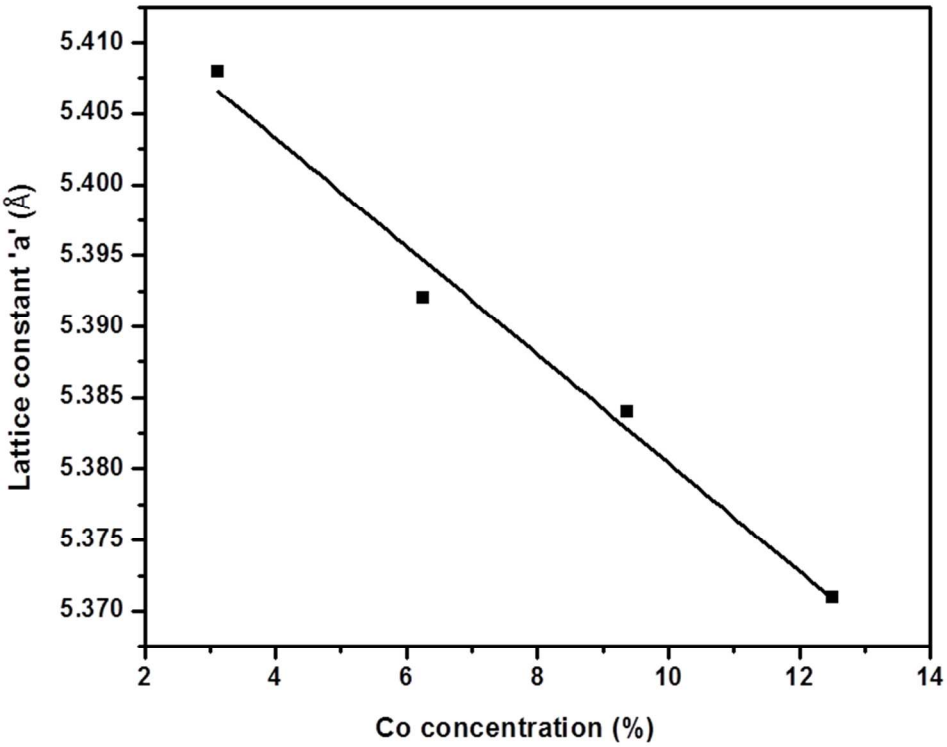

Figure 12: Variation in theoretically calculated lattice constant 'a' as a function of cobalt concentration

It is well known that when a semiconductor is doped with transition metal atoms, it is the p-d hybridization between the p-orbital of host and d-orbital of the dopant material that govern the ferromagnetic coupling in the system. In the present case, the p–d hybridization between the Co 3d and S 3p has vital role since it is the short-range interaction. The energy of ZnCoS system is decreased by p–d hybridization at the ferromagnetic state while at antiferromagnetic coupling state the total energy remains unchanged. By the p–d hybridization interaction, a moment is established around cobalt atom and then by RKKY interaction, the ferromagnetic coupling state between the atoms of cobalt is formed. Spin-polarized local DOS and particularly the interaction effects in the DOS introduced by the hybridization with the wave functions of neighboring atoms are of much importance. The hybridization with the un-occupied majority and occupied minority 'd' states of Co acts like a magnetic field on the conduction band states which induces a spin

polarization in the host. The spin polarized partial densities of states of cobalt are given in Figure 13. The magnetic moments found in case of cobalt doping are presented in Table 2.

Table 2: Structural and magnetic properties of ZnS:Co (3.125, 6.25, 9.375 and 12.50 at.%) supercells

Models	Supercell	Concentration of Co (at %)	Lattice constant (Å)	Moment (μB)
1	$Zn_{31}Co_1S_{32}$	3.125	5.408	2
2	$Zn_{30}Co_2S_{32}$	6.250	5.392	3
3	$Zn_{29}Co_3S_{32}$	9.375	5.384	4
4	$Zn_{28}Co_4S_{32}$	12.500	5.371	4

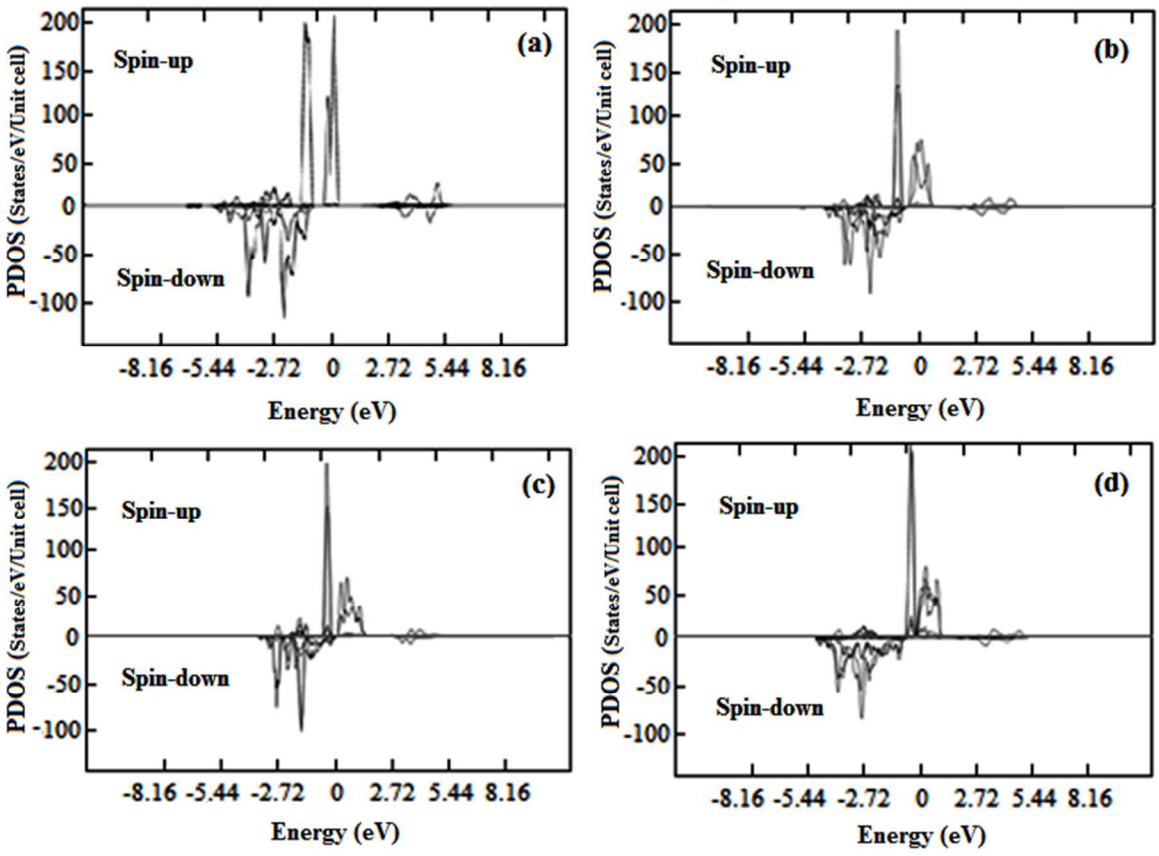

Figure 13: Spin polarized partial density of states (PDOS) for cobalt (a) 3.125% Co, (b) 6.25% Co, (c) 9.375% Co and (d) 12.50% Co.

Earlier study on "first-principles theory of dilute magnetic semiconductors" by Sato *et al.* revealed that the magnetic moment calculated for 5% cobalt doped ZnS system is 3μB[38] which is in well agreement with that calculated in present study. Due to incorporation of cobalt, empty or partially filled majority states at the Fermi level are introduced keeping the minority states occupied due to double exchange (RKKY) interactions. This suggests that cobalt doping leads to 100% spin polarization and results in half metallicity in ZnS. The asymmetry in total density of states (TDOS) after cobalt doping in ZnS is shown in Figure 14.

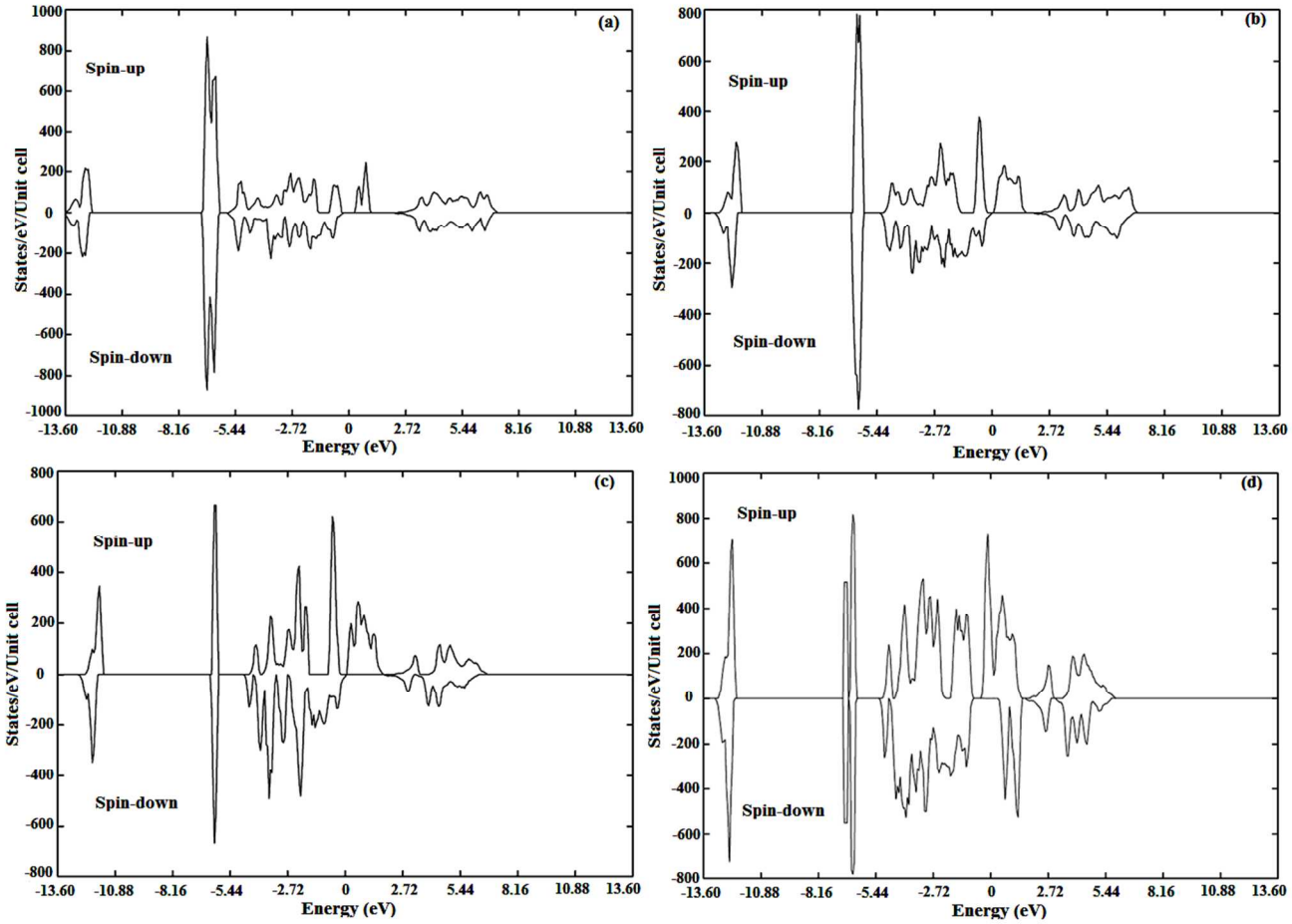

Figure 14: Spin polarized total density of states (TDOS) for ZnCoS (a) 3.125% Co, (b) 6.25% Co, (c) 9.375% Co and (d) 12.50% Co.

5. CONCLUSIONS

Cobalt doped ZnS thin films have been deposited onto glass substrates by chemical bath deposition. The p-XRD showed broad peaks correspond to the cubic phase of ZnS with only slight shift in 2θ values as expected. Cobalt doping resulted in a slight change of lattice parameters of ZnS; the extent of change depended on the concentration of cobalt in ZnS lattice. SEM images showed the clusters of spherical nanoparticles with almost equal size for all the doping concentrations. TEM/HRTEM/SAED analyses confirmed the deposition of polycrystalline cubic phase of ZnS. UV/Vis and PL studies revealed that the deposited thin films are highly transparent in visible region in addition to enhanced green emission at higher cobalt concentrations. Magnetic analysis revealed the presence of room temperature ferromagnetism in all the samples. Theoretical investigations were consistent with the experimental data in all aspects in addition to the observation of half metallicity in cobalt doped ZnS clusters. These films have potential applications in advanced optoelectronic and spintronic devices.

ACKNOWLEDGMENT

M S Akhtar would like to acknowledge the Higher Education Commission (HEC) of Pakistan for providing financial support as indigenous scholarship (Grant no.17-5-4(Ps4-264)/HEC/Sch./2007) in Batch-IV and IRSIP scholarship (Grant no.1-8/HEC/HRD/ 2013/2503).

REFERENCES

1. I. Polat, S. Aksu, M. Altunbas and E. Bacaksiz, *Mater Chem Phys*, 2011, **130**, 800-805.
2. S. P. Patel, J. C. Pivin, M. K. Patel, J. Won, R. Chandra, D. Kanjilal and L. Kumar, *J Magn Magn Mater*, 2012, **324**, 2136-2141.
3. L. Ma and W. Chen, *Nanotechnology*, 2010, **21**, 385604.
4. L. Liu, L. Yang, Y. Pu, D. Xiao and J. Zhu, *Mater Lett*, 2012, **66**, 121-124.
5. S. Sambasivam, D. P. Joseph, J. G. Lin and C. Venkateswaran, *J Solid State Chem*, 2009, **182**, 2598-2601.
6. W. J. Fang, Y. S. Liu, B. Z. Guo, L. Peng, Y. B. Zhong, J. C. Zhang and Z. J. Zhao, *J Alloy Compd*, 2014, **584**, 240-243.
7. L. J. Tang, G. F. Huang, Y. Tian, W. Q. Huang, M. G. Xia, C. Jiao, J. P. Long and S. Q. Zhan, *Mater Lett*, 2013, **100**, 237-240.
8. M. S. Akhtar, M. A. Malik, S. Riaz, S. Naseem and P. O'Brien, *Mat Sci Semicon Proc*, 2015, **30**, 292-297.
9. B. Poornaprakash, D. A. Reddy, G. Murali, N. M. Rao, R. P. Vijayalakshmi and B. K. Reddy, *J Alloy Compd*, 2013, **577**, 79-85.
10. C. S. Pathak, M. K. Mandal and V. Agarwala, *Mat Sci Semicon Proc*, 2013, **16**, 467-471.
11. V. Ramasamy, K. Praba and G. Murugadoss, *Spectrochim Acta A*, 2012, **96**, 963-971.
12. M. Jadraque, A. B. Evtushenko, D. Avila-Brande, M. Lopez-Arias, V. Loriot, Y. G. Shukhov, L. S. Kibis, A. V. Bulgakov and M. Martin, *J Phys Chem C*, 2013, **117**, 5416-5423.
13. Q. Hou, K. Chen, H. Zhang, Y. Li, H. Liu, X. Dong, Y. Huang and Q. Li, *Journal of Physics: Conference Series*, 2013, **430**, 012076.
14. X. B. Chen, N. Yang, X. F. Liu and R. H. Yu, *Phys Scripta*, 2013, **88**, 035703.
15. L. Zhang, D. Z. Qin, G. R. Yang and Q. X. Zhang, *Chalcogenide Lett*, 2012, **9**, 93-98.
16. L. Y. Liu, L. Yang, Y. T. Pu, D. Q. Xiao and J. G. Zhu, *Mater Lett*, 2012, **66**, 121-124.
17. M. A. Malik, M. Motevalli and P. O'Brien, *Inorg Chem*, 1995, **34**, 6223-6225.
18. N. Revaprasadu, M. A. Malik, P. O'Brien and G. Wakefield, *J Mater Res*, 1999, **14**, 3237-3240.
19. M. A. Malik, M. Motevalli, J. R. Walsh and P. Obrien, *Organometallics*, 1992, **11**, 3136-3139.

20. A. A. Memon, M. Afzaal, M. A. Malik, C. Q. Nguyen, P. O'Brien and J. Raftery, *Dalton T*, 2006, 4499-4505.
21. D. J. Binks, S. P. Bant, D. P. West, P. O'Brien and M. A. Malik, *J Mod Optic*, 2003, **50**, 299-310.
22. C. Q. Nguyen, A. Adeogun, M. Afzaal, M. A. Malik and P. O'Brien, *Chem Commun*, 2006, 2182-2184.
23. M. A. Malik, M. Motevalli, T. Saeed and P. Obrien, *Adv Mater*, 1993, **5**, 653-654.
24. A. Panneerselvam, C. Q. Nguyen, M. A. Malik, P. O'Brien and J. Raftery, *J Mater Chem*, 2009, **19**, 419-427.
25. H. N. Dong, B. Zhang, P. D. Chen, C. L. Zhang and J. Liu, *Chinese J Inorg Chem*, 2012, **28**, 1447-1452.
26. J. H. Zhang, J. W. Ding, J. X. Cao and Y. L. Zhang, *J Solid State Chem*, 2011, **184**, 477-480.
27. H. X. Chen, D. N. Shi and J. S. Qi, *J Appl Phys*, 2011, **109**.
28. W. Kohn and L. J. Sham, *Physical Review*, 1965, **140**, A1133-A1138.
29. P. Hohenberg and W. Kohn, *Physical Review*, 1964, **136**, B864-B871.
30. J. P. Perdew, K. Burke and M. Ernzerhof, *Physical Review Letters*, 1996, **77**, 3865-3868.
31. A. Bayer, D. S. Boyle and P. O'Brien, *J Mater Chem*, 2002, **12**, 2940-2944.
32. J. Tauc and A. Menth, *J Non-Cryst Solids*, 1972, **8–10**, 569-585.
33. S. H. Mohamed, *Journal of Physics D: Applied Physics*, 2010, **43**, 035406.
34. P. Yang, M. Lü, D. Xü, D. Yuan, C. Song and G. Zhou, *J Phys Chem Solids*, 2001, **62**, 1181-1184.
35. R. Sarkar, C. S. Tiwary, P. Kumbhakar and A. K. Mitra, *Physica B: Condensed Matter*, 2009, **404**, 3855-3858.
36. J. K. Furdyna, *J Appl Phys*, 1988, **64**, R29-R64.
37. R. A. Stern, T. M. Schuler, J. M. MacLaren, D. L. Ederer, V. Perez-Dieste and F. J. Himpsel, *J Appl Phys*, 2004, **95**, 7468-7470.
38. K. Sato, L. Bergqvist, J. Kudrnovský, P. H. Dederichs, O. Eriksson, I. Turek, B. Sanyal, G. Bouzerar, H. Katayama-Yoshida, V. A. Dinh, T. Fukushima, H. Kizaki and R. Zeller, *Reviews of Modern Physics*, 2010, **82**, 1633-1690.

Graphical abstract:

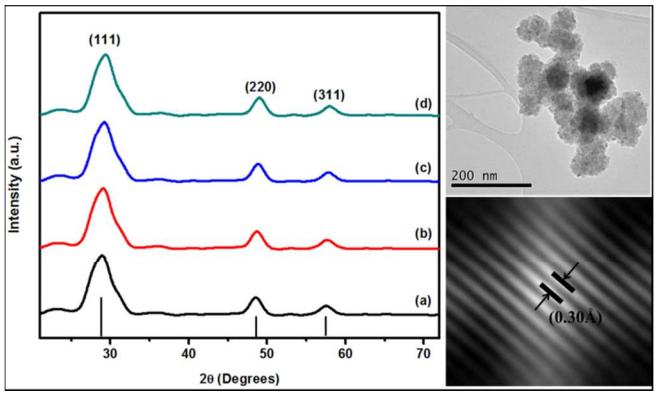

An optimized growth of nanocrystalline cobalt doped ZnS thin films on glass substrates was carried out by CBD method. The structural, morphological, magnetic and optical properties of deposited thin films have been studied.